

Random acceleration noise on Stern-Gerlach Interferometry in a Harmonic Trap

Sneha Narasimha Moorthy^{1,2}, Andrew Geraci³, Sougato Bose⁴, and Anupam Mazumdar⁵

¹*School of Physical Sciences,
National Institute of Science Education and Research,
Jatni 752050, India*

²*Homi Bhabha National Institute,
Training School Complex,
Anushaktinagar, Mumbai 400094, India*

³*Center for Fundamental Physics,
Department of Physics and Astronomy,
Northwestern University,
2145 Sheridan Road, Evanston, IL, USA*

⁴*Department of Physics and Astronomy,
University College London, Gower Street,
WC1E 6BT London, United Kingdom*

⁵*Van Swinderen Institute, University of Groningen,
9747 AG Groningen, The Netherlands*

(Dated: February 26, 2026)

We analyze decoherence in a one-loop Stern–Gerlach–type matter-wave interferometer for a massive nanoparticle embedded with a nitrogen vacancy (NV)-centred nanodiamond evolving under an effective harmonic-oscillator dynamics in a magnetic-field gradient. We assume that the Stern–Gerlach interferometer is subjected to a random acceleration noise external to the system. This could be along the direction of the superposition at an angle which can be varied. We quantify dephasing from two noise channels: fluctuations in the external acceleration $a(t)$ magnitude and direction as specified by the tilt angle $\theta_0(t)$ between the superposition axis and the acceleration. At the level of the action, we treat these two external noise as stochastic inputs, and compute the resulting stochastic arm-phase difference, and obtain the dephasing rate Γ using the Wiener–Kinchin theorem. For a white noise and a coherence target $\Gamma\tau \leq 1$ and by assuming that we finish the one-loop interferometer within $\tau = 2\pi/\omega_0 \simeq 0.015$ s, for a reasonable choice of the magnetic field gradient, $\eta_0 = 6 \times 10^3$ T m⁻¹ and mass of the nanodiamond, $m = 10^{-15}$ kg) to create a superposition size of $\Delta x \sim 1$ nm. We find $\sqrt{\mathcal{S}_{aa}} \lesssim \mathcal{O}(10^{-11})$ ms⁻² Hz^{-1/2} even if we take the external acceleration, $a = 0$ ms⁻² and $\theta_0 = 0^\circ$ (along the direction of the superposition), and $\sqrt{\mathcal{S}_{\theta\theta}} \lesssim \mathcal{O}(10^{-10})$ rad Hz^{-1/2} for $a = g = 9.81$ ms⁻² and $\theta_0 = 0^\circ$ (superposition direction is perpendicular to the Earth’s gravity). We have also found an operating regime where the acceleration noise can be minimized by either varying θ_0 or a for a fixed set of other experimental parameters.

I. INTRODUCTION

Matter-wave interferometers are becoming increasingly sophisticated to test fundamental physics involving quantum-mechanical principles for heavy masses [1–3], including the large spatial superposition [4–9], and states of a massive object [10–14]. By increasing the mass, we become more sensitive to the gravitational interaction, leading to a recent protocol to test the quantum nature of the gravitational interaction with matter by keeping two adjacent matter-wave interferometers and studying quantum features such as entanglement to witness the quantum nature of gravity, known as quantum gravity induced entanglement of matter (QGEM) [15–17]. Similar to the light-bending experiment due to gravity, one proposed test is to examine how the quantum-gravitational interaction can lead to entanglement between matter and a photon via the exchange of a virtual graviton [18]. Similarly, with the help of matter wave interferometers, one can probe the Kaluza-Klein theory of massive graviton and entanglement [19], non-local gravitational interac-

tions [20], and test the weak equivalence principle via witnessing entanglement [21, 22].

There are many challenges to overcome before we can reach the precision to create a large macroscopic quantum superposition. There are many sources of decoherence for massive quantum systems [23, 24] due to random external fluctuations in ambient temperature/pressure [24–28], systematics related to initialization [29], current/magnetic field fluctuations [30, 31], external dipoles [32], voltage [33], random accelerations and gravity gradients [34, 35]. There are phonon-induced noise [36–38], and fluctuation in the spin degrees of freedom during the dynamics of rotation of the rigid body [39–44], all leading to dephasing and decoherence, see [23, 45, 46], and loss of contrast [47–50].

One particularly popular platform for creating large spatial superposition is within diamagnetically levitated nanoparticle with a defect such as the nitrogen vacancy (NV)-centred nanodiamond, see for a review on NV properties of nanodiamond [51]. For NV-centered nanodiamonds, it is possible to create a spin superposition of $|+1\rangle$ and $|-1\rangle$ states. It is also possible to cool a

nanoparticle to a motional ground state in optical and in ion traps, see [52–56], and nanodiamonds in a diamagnetic traps, see [57]. Once motionally cooled the idea is to apply the Stern-Gerlach inhomogeneous magnetic field on the spin of NV [7, 50] to separate the centre of mass motion of the nanodiamond onto left and right trajectories, before bringing them together to perform one-loop interferometer, thereby creating a Schrödinger cat state.

The current paper analyses a small part of the whole lot of noise budget, but a significant one from the experimental perspective. The current analysis focuses on characterizing the dephasing introduced by noise in an external acceleration field, like external jitters/vibrations in the vicinity of the experiment by modeling it using classical stochastic processes at the Lagrangian level. We consider the impact of Gaussian white noise on the phase evolution of the interferometric superposition. Additionally, we analyze the dephasing due to fluctuations in the tilt angle between the superposition axis and the external acceleration field. We obtain bounds on the noise parameters including the power spectral density (PSD) describing the acceleration and tilt fluctuation statistics. We also note that, unlike the tilt fluctuations [29] and magnetic noise fluctuations, [30, 31], that can be controlled experimentally using finer precision, the gravitational field fluctuation is a true environmental fluctuation, whose origin can be seismic [58], or a random acceleration noise [34], similar in the context of gravitational wave detectors [59, 60], see for a review [61].

II. SETUP

We consider a massive nanodiamond of mass $m \sim 10^{-15}$ kg with a single nitrogen–vacancy (NV) center, whose ground-state electronic spin is $S = 1$ ¹. We prepare the NV spin in an equal superposition of the $|m_x = +1\rangle$ and $|m_x = -1\rangle$ eigenstates of S_x , and use a spin-dependent force to spatially separate the nanoparticle’s centre-of-mass wavepacket into two branches, thereby entangling spin and position degrees of freedom. We shall focus only on the dynamics along the x-axis (one-dimensional matter-wave interferometer), along which spatial superposition is intended to be created.

We consider a general case when the axis of spatial separation makes an arbitrary angle with the direction of acceleration due to some external force like vibration of a table and gravitational acceleration. The corresponding Lagrangian for each of the arms ($j \in \{R, L\}$) of the interferometer is [64, 65]:

$$L_j = \frac{1}{2}m\dot{x}_j^2 + \frac{\chi_\rho m}{2\mu_0}B_{xj}^2 - \hbar\gamma_e S_{xj} B_{xj} - \hbar D S_{NV}^2 + m a x_j \cos \theta_0 \quad (1)$$

¹The choice of the mass is based on the QGEM experiment, see [62, 63]. We can vary the mass in our analysis.

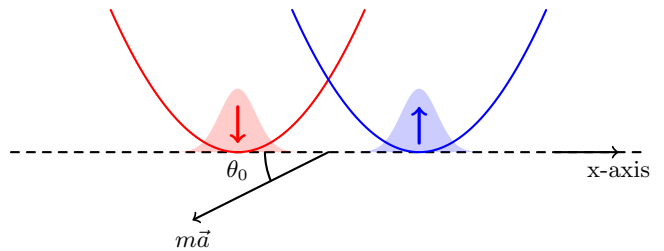


FIG. 1: Schematic of a nanoparticle interferometer in a tilted spin-dependent harmonic potential. The magnetic-field gradient produces spin-dependent harmonic oscillator potentials. External random acceleration is acting at an angle θ_0 to the axis of spatial superposition. The gaussian wavepackets represent the states constituting the two interferometer arms.

where R and L refer to the right and left arms of the interferometer, and $S_{xR} = 1$ and $S_{xL} = -1$. The first term is the kinetic term, the second term is the diamagnetic induced contribution, where $\chi_\rho = -6.286 \times 10^{-9} \text{ m}^3 \text{ kg}^{-1}$ (for nanodiamond) represents the mass magnetic susceptibility, $\mu_0 = 4\pi \times 10^{-7} \text{ H m}^{-1}$ is the magnetic permeability, $\hbar = 1.05 \times 10^{-34} \text{ kg m}^2 \text{ s}^{-1}$ is the reduced Planck’s constant, $\gamma_e = 1.761 \times 10^{11} \text{ s}^{-1} \text{ T}^{-1}$ is the electron gyromagnetic ratio. The external magnetic field at x_j is given by B_{xj} ². The third term indicates the spin-magnetic field coupling, $\vec{\mu}_S \cdot \vec{B}$ where $\vec{\mu}$ is the spin magnetic moment³. The parameter D denotes the zero-field splitting, which for NV centers is $D = 2.87 \text{ GHz}$ [66]. The last term in the Lagrangian is introduced by the axis of spatial superposition, making an angle θ_0 with respect to the direction of acceleration $\vec{a} = (a_x, a_y, a_z) \equiv a\hat{a}$. In other words, since we have considered the interferometer axis along x , i.e. $a_x = a \cos \theta_0 = \hat{x} \cdot \vec{a}$

To study the effect of fluctuations in the gravitational acceleration, we shall use a simple model of the interferometer setup, assuming the magnetic field to be $B_x = B_0 + \eta_0 x$, where B_0 is the biased magnetic field. Thus, the Lagrangian becomes:

$$L_j = \frac{1}{2}m\dot{x}_j^2 - \frac{1}{2}m\omega_0^2 x_j^2 - C_j \eta_0 x_j + \frac{\chi_\rho m}{2\mu_0} B_0^2 - S_{xj} \hbar \gamma_e B_0 - \hbar D S_{NV}^2 + m a x_j \cos \theta_0, \quad (2)$$

where,

$$C_j = \left(S_{xj} \hbar \gamma_e - \frac{\chi_\rho m}{\mu_0} B_0 \right) \quad (3)$$

²The dependence of B_{xj} on the interferometer arm accounts for non-uniform magnetic fields of the form: $B_x \simeq B_0 + \eta_1 x$.

³ $S \cdot B$ term gives rise to a spin-dependent potential. This allows for entangling spin and position degrees of freedom, thus creating the two arms of the interferometer.

and the characteristic frequency ω_0 is defined as:

$$\omega_0 = \left(-\frac{\chi_\rho}{\mu_0} \right)^{1/2} \eta_0. \quad (4)$$

For a one-loop interferometer, the time for a single run of the experiment would be: $\tau = 2\pi/\omega_0$. In the analysis of the current paper, we consider a one-loop interferometer. The equation of motion is as follows:

$$m\ddot{x}_j(t) = -m\omega_0^2 x_j(t) - C_j \eta_0 + ma \cos \theta_0 \quad (5)$$

Imposing $x_j(0) = 0$ and $\dot{x}(0) = 0$, we get:

$$x_j(t) = \frac{C_j \eta_0 - ma \cos \theta_0}{m\omega_0^2} (\cos(\omega_0 t) - 1) \quad (6)$$

We define:

$$\tilde{C}_j = C_j \eta_0 - ma \cos \theta_0 \quad (7)$$

then the trajectory of each arm of the interferometer is given by:

$$x_j(t) = \frac{\tilde{C}_j}{m\omega_0^2} (\cos(\omega_0 t) - 1) \quad (8)$$

The maximum spatial superposition size (Δx_{\max}) is obtained for $t = \frac{\pi}{\omega_0}$:

$$\begin{aligned} \Delta x_{\max} &= \left| x_R \left(\frac{\pi}{\omega_0} \right) - x_L \left(\frac{\pi}{\omega_0} \right) \right| = 2 \frac{\tilde{C}_R - \tilde{C}_L}{m\omega_0^2} \\ &= 4 \frac{\hbar \gamma_e \eta_0}{m\omega_0^2} \end{aligned} \quad (9)$$

Hence, the superposition size doesn't depend on the magnetic field offset B_0 or on the external acceleration parameters a and θ_0 . However, the superposition size does depend on mass as shown in Fig.2. Note that the mass will also affect the dephasing parameters in both θ and acceleration.

To study the effect of fluctuations in the acceleration a on dephasing the interferometer, we briefly recap noise analysis in the following section.

III. NOISE ANALYSIS

We first consider a general Lagrangian of the form:

$$\mathcal{L}_j = \frac{1}{2} m v_j^2 - A_j x_j^2 - B_j x_j - C_j, \quad \text{where } j \in \{L, R\}. \quad (10)$$

and j represents the right and left arms of the interferometer. We consider a noise source, $\delta\zeta(t)$, which leads to fluctuations in the coefficients of the Lagrangian, for instance $A_j \rightarrow A_j + \delta A_j(t)$ if A_j depends on ζ . The modified Lagrangian gives rise to modified equations of motion and hence modified trajectories, say $x_j \rightarrow x_j + \delta x_j$. If the statistics of the noise are known, we can compute the dephasing rate using the following method, see for instance [30]:

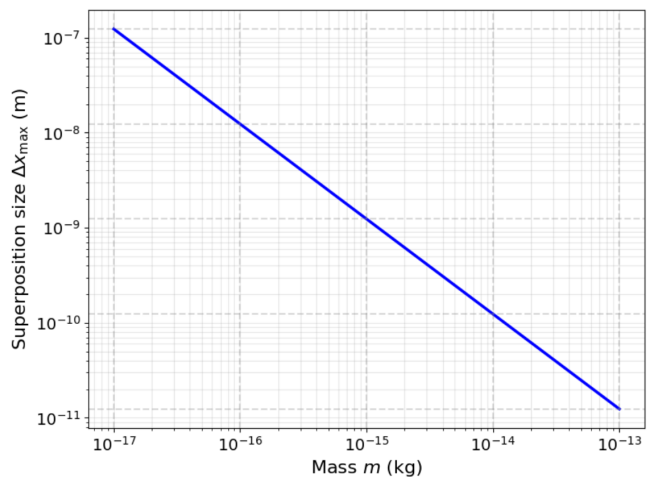


FIG. 2: The graph depicts the variation of the maximum superposition size achievable in a harmonic potential with variation of the mass of the nanoparticle in a Stern-Gerlach-type interferometer for a set of parameters given by: $\eta_0 = 6 \times 10^3 \text{Tm}^{-1}$, $m = 10^{-15} \text{kg}$.

- Compute the relative phase between the two arms of the interferometer: $\Delta\phi = \frac{1}{\hbar} \int_{t_i}^{t_f} (\mathcal{L}_R - \mathcal{L}_L) dt$.
- Identify noise sources affecting coefficients A_j , B_j , C_j , introducing time-dependent fluctuations $\delta A_j(t)$, $\delta B_j(t)$, $\delta C_j(t)$. Characterise their statistical properties (generally in the frequency space, including power spectral density $\mathcal{S}(\omega)$).
- Derive equations of motion (EOM) for trajectories x_j (noiseless) and x_j^{tot} (with noise). Compute trajectory deviation: $\delta x_j = x_j^{\text{tot}} - x_j$.
- Calculate the phase fluctuation due to noise:

$$\begin{aligned} \delta\phi &= \frac{1}{\hbar} \int_{t_i}^{t_f} \left[(\delta A_R x_R^2 - \delta A_L x_L^2) \right. \\ &\quad \left. + (\delta B_R x_R - \delta B_L x_L) + (\delta C_R - \delta C_L) \right] dt \\ &\quad + \frac{1}{\hbar} \int_{t_i}^{t_f} \left[(A_R \delta x_R^2 - A_L \delta x_L^2) \right. \\ &\quad \left. + (B_R \delta x_R - B_L \delta x_L) \right] dt \end{aligned} \quad (11)$$

- If the statistical properties of the noise considered are given in the frequency space, then transform equation eq.(11) to frequency space. Evaluate the dephasing rate, see [67]:

$$\Gamma = \lim_{\tilde{\tau} \rightarrow \infty} \frac{1}{\tilde{\tau}} E[(\delta\phi(\tilde{\tau}))^2] \quad (12)$$

where $E[\cdot]$ denotes ensemble average and $\delta\phi(\tilde{\tau})$ refers to the phase when the noise source lasts for a time $\tilde{\tau}$.

- The dephasing rate is given by [30]:

$$\Gamma \leq \int_0^\infty \mathcal{S}(\omega) \left| \sum_i \sqrt{F_i(\omega)} \right|^2 d\omega \quad (13)$$

where $\mathcal{S}(\omega)$ is the noise power spectral density, which from the Wiener-Khinchin theorem [68, 69] is defined as ⁴:

$$\mathcal{S}(\omega) = \lim_{\bar{\tau} \rightarrow \infty} \frac{1}{\bar{\tau}} E[\delta\tilde{\zeta}_{\bar{\tau}}(\omega)\delta\tilde{\zeta}_{\bar{\tau}}^*(\omega)]. \quad (14)$$

- We compute the effective transfer functions ⁵ $F_i(\omega)$, e.g., $F_1(\omega) \propto \left| \int_{t_i}^{t_f} (x_R - x_L) e^{i\omega t} dt \right|^2$, using the expression obtained from eq.(12).

The statistical properties of noise are generally characterised in the frequency space as the mean of the noise amplitudes, while second order correlation giving rise to the power spectral density and higher order correlations ⁶. In the case of Gaussian noise, we have only the first two correlation functions which are independent:

$$\delta\tilde{\zeta}(\omega) = \frac{1}{2\pi} \int_{-\infty}^{\infty} \delta\zeta(t) e^{i\omega t} dt$$

$$E[\delta\tilde{\zeta}(\omega)] = 0 \quad (15)$$

$$E[\delta\tilde{\zeta}(\omega)\delta\tilde{\zeta}^*(\omega')] = \mathcal{S}_{\zeta\zeta}(\omega)\delta(\omega - \omega') \quad (16)$$

where $E[\cdot]$ denotes ensemble average. $\mathcal{S}_{\zeta\zeta}(\omega)$ is known as the power spectral density of the noise [67].

In this paper, we present the dephasing rate due to fluctuations in system parameters, including acceleration (a) and tilt angle (θ_0). We assume white noise statistics, where the power spectral density is a constant:

$$E[\delta\tilde{\zeta}(\omega)] = 0, \quad \mathcal{S}_{\zeta\zeta}(\omega) \equiv \mathcal{S}_{\zeta\zeta} = \text{const.} \quad (17)$$

A. Coherence measure

Our aim is to compute the bound on the noise parameter $\mathcal{S}_{\xi\xi}$ to obtain a minimum coherence required for spin readout at the end of the interferometer. To obtain quantitative bounds on noise we need to quantify coherence, which is given by:

$$\text{Coherence measure} = \text{CM} = e^{-\Gamma\tau} \in [0, 1] \quad (18)$$

⁴The notation we use is: $\delta\tilde{\zeta}_{\bar{\tau}}(\omega) = \frac{1}{2\pi} \int_{-\bar{\tau}}^{\bar{\tau}} \delta\zeta(t) e^{i\omega t} dt$

⁵We note that the units of the effective transfer functions is the inverse of that of the power spectral density. The units of the PSD depends only on the parameter being perturbed, $\delta\xi(t)/\text{noise source}$.

⁶The Fourier space contains positive and negative frequencies. Mathematically, both are required to describe an arbitrary complex function in the time domain. To obtain a real function in the time domain, the Fourier conjugate must follow: $\tilde{\zeta}(-\omega) = \tilde{\zeta}^*(\omega)$. Thus, the negative-frequency components are not independent.

where Γ is the dephasing rate and τ is the time required to complete one-loop interferometer, i.e. one run of the experiment. Note that when the dephasing rate is zero, the coherence measure is unity, and when the dephasing rate tends to arbitrarily large values, the coherence measure vanishes. According to eq.(18), the average decoherence time is:

$$\langle T_{\text{decoh}} \rangle = \int_0^\infty \text{CM}(\tau) d\tau = \int_0^\infty e^{-\Gamma\tau} d\tau = \Gamma^{-1} \quad (19)$$

One generally imposes that the average decoherence time $1/\Gamma$ to be greater than the time of the experiment:

$$\Gamma^{-1} > \tau \implies \Gamma\tau < 1 \implies e^{-\Gamma\tau} > e^{-1} \quad (20)$$

B. Accounting for multiple sources of fluctuations

In an experimental setup, there are multiple sources of fluctuations. One can obtain the upper bound on the dephasing due all of them by using the triangle inequality: Let $\{\delta\zeta_1, \delta\zeta_2, \dots, \delta\zeta_n\}$ be the set of fluctuating parameters in the system. Let $\{\Gamma_1, \Gamma_2, \dots, \Gamma_n\}$ be the respective dephasing rates due to each of the fluctuating parameters considered. Then, the upper bound on the total dephasing rate is:

$$\Gamma \leq \sqrt{\Gamma_1^2 + \Gamma_2^2 + \dots + \Gamma_n^2} \quad (21)$$

We now compute the dephasing rate introduced by fluctuations in acceleration, and compute the bound on the noise parameters for the specific case of fluctuations when $a = g$, Earth's gravitational acceleration in a laboratory.

IV. FLUCTUATIONS IN ACCELERATION

Consider the fluctuation: $a \rightarrow a + \delta a_j(t)$. We consider the fluctuation in the acceleration, $\delta a_j(t)$, to be a function of space, and hence a function of the interferometer arms, $j \in \{R, L\}$. The modified Lagrangian is:

$$\delta L_j = m\dot{x}_j\delta\dot{x}_j - m\omega_0^2 x_j\delta x_j - C_j\eta_0\delta x_j + ma\delta x_j \cos\theta_0 + m\delta a_j x_j \cos\theta_0 \quad (22)$$

where δx_j is the fluctuation introduced in each trajectory due to the fluctuations in the acceleration ⁷. The corresponding fluctuation in the phase, following eq.(11) is:

$$\delta\phi = \frac{1}{\hbar} \int_0^\tau (\delta L_R - \delta L_L) dt \quad (23)$$

⁷ $x_j + \delta x_j$ is the change trajectory obtained from the equations of motion derived from the modified Lagrangian, $L_j + \delta L_j$.

where we consider $\tau = 2\pi/\omega_0$ indicating a one loop interferometer, where ω_0 is as defined in eq.(4). In [70], it was shown that trajectory and velocity in Lagrangians like eq.(2) does not contribute to the dephasing in a one-loop interferometer. This is explicitly shown in Appendix A. Hence, the phase fluctuation arises only from the last term in eq.(22):

$$\delta\phi_a = \frac{m \cos \theta_0}{\hbar} \int_0^\tau dt \left(\delta a_R(t) x_R(t) - \delta a_L(t) x_L(t) \right) \quad (24)$$

Now, we Fourier transform the fluctuations of the acceleration into the frequency basis:

$$\delta a_j(t) = \int_{-\infty}^{\infty} d\omega \delta \tilde{a}_j(\omega) e^{i\omega t}. \quad (25)$$

Further, we will consider an uncorrelated Gaussian noise statistics, as given in eqs.(15)-(16), in both the arms of the interferometer:

$$E[\delta \tilde{a}_j(\omega)] = 0 \quad (26)$$

$$E[\delta \tilde{a}_j^*(\omega) \delta \tilde{a}_{j'}(\omega')] = \mathcal{S}_{aa_j}(\omega) \delta(\omega - \omega') \delta_{jj'} \quad j, j' \in \{L, R\}$$

where $\mathcal{S}_{aa_j}(\omega)$ is the PSD of the noise considered. By considering $\delta_{jj'}$ term in eq.(26), we are assuming that the acceleration fluctuations experienced by one arm of the interferometer are uncorrelated to those in the other arm⁸. We will strictly assume that the PSD $\mathcal{S}_{aa_j}(\omega)$ is the same for both the arms, $\mathcal{S}_{aa}(\omega)$, in our analysis.

The second order correlation of the phase fluctuation is calculated by imposing the statistics and the equations of motion, i.e. eqs.(26),(8), and using eqs.(24),(25), to compute the dephasing rate, Γ_{aa} upto first order perturbations in the acceleration, see eq.(12):

$$\begin{aligned} \Gamma_{aa} &= \lim_{\tilde{\tau} \rightarrow \infty} \frac{1}{\tilde{\tau}} E[\delta \phi_a^*(\tilde{\tau}) \delta \phi_a(\tilde{\tau})] = E[\delta \phi_a^* \delta \phi_a] \\ &= \frac{\cos^2 \theta_0}{\omega_0^4} (\tilde{C}_R^2 + \tilde{C}_L^2) \int_{-\infty}^{\infty} d\omega \mathcal{S}_{aa}(\omega) \int_0^\tau dt' \int_0^\tau dt \\ &\quad \times e^{i\omega(t-t')} (\cos(\omega_0 t) - 1) (\cos(\omega_0 t') - 1) \\ &= 4 \frac{\cos^2 \theta_0}{\omega_0^5} (\tilde{C}_R^2 + \tilde{C}_L^2) \times \int_{-\infty}^{\infty} d\xi \mathcal{S}_{aa}(\omega_0 \xi) \frac{\sin^2(\pi \xi)}{\xi^2 (\xi^2 - 1)^2} \end{aligned} \quad (27)$$

where $\xi = \omega/\omega_0$. By using the expression for the trajectories from eq.(8), and comparing the above with the

⁸Correlation of noise statistics between the two arms will contribute to dephasing. It is likely that the two arms will have correlated noise statistics since the source of fluctuation is the same. If we assume the noise source is far from the interferometer compared to the distance between the interferometer arms, then the correlation is likely positive, leading to a decrease in the dephasing rate. However, we are not dealing with any particular model for the noise source, and hence compute the dephasing for the uncorrelated case to obtain the upper bound on the dephasing rate given the system parameters. Refer to Appendix.B.

form in eq.(13), we can obtain the effective transfer function up to first order in acceleration, which is given by:

$$\begin{aligned} |F_{a,\text{eff}}(\omega)|^2 &= \frac{\cos^2 \theta_0}{\omega_0^4} (\tilde{C}_R^2 + \tilde{C}_L^2) \int_0^\tau dt' \int_0^\tau dt \\ &\quad \times (\cos(\omega_0 t) - 1) (\cos(\omega_0 t') - 1) e^{i\omega(t-t')} \\ |F_{a,\text{eff}}(\omega_0 \xi)|^2 &= \frac{4 \cos^2 \theta_0}{\omega_0^6} (\tilde{C}_R^2 + \tilde{C}_L^2) \frac{\sin^2(\pi \xi)}{\xi^2 (\xi^2 - 1)^2}. \end{aligned} \quad (28)$$

To understand the susceptibility of the system to different frequencies of fluctuations in acceleration, we analyse the transfer function given in eq.(28). Note that the coefficient of $f_{aa}(\xi) = \sin^2(\pi \xi)/(\xi^2 (\xi^2 - 1)^2)$ is a constant for a given set of system parameters like θ_0 , a , ω_0 , etc. Hence, to understand the bandwidth of frequencies that can affect the system, it is sufficient to look at the behaviour of $f_{aa}(\xi)$. From Fig.3, we can understand that

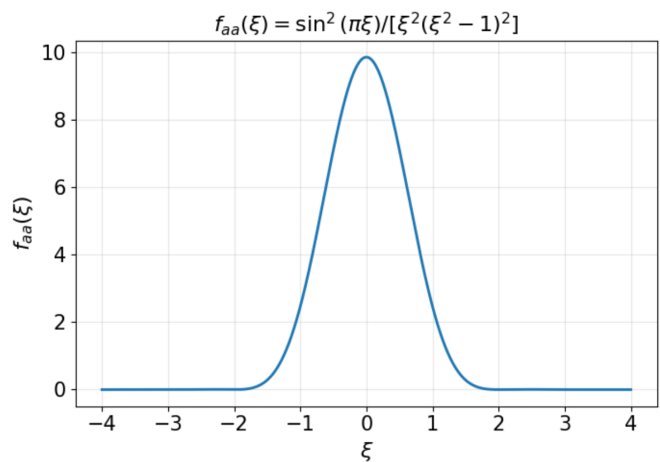


FIG. 3: The plot shows the frequency response of the interferometer to acceleration fluctuations. The horizontal axis is the dimensionless quantity $\xi = \omega/\omega_0$, where ω is the angular frequency of the noise source and ω_0 is the characteristic angular frequency of the harmonic oscillator. The vertical axis shows $f_{aa}(\xi)$, the frequency-dependent weighting factor appearing in the acceleration-noise transfer function eq.(28). Larger $f_{aa}(\xi)$ indicates greater sensitivity to perturbations at that normalised frequency.

when the noise source is white, i.e., where the PSD is constant over all frequencies, the dephasing rate involving the product of the PSD and the transfer function makes it integrable over the whole range of frequencies. We further note that the values of ξ contributing significantly to the transfer function is $|\xi| \leq 1 \implies |\omega| \leq |\omega_0|$.

In many experiments, one can argue that when the experimental time duration is $\tau = 2\pi/\omega_0$, noise components with frequencies much less than $\omega < \omega_0$ can be neglected, since they are effectively constant over this time interval. This reasoning is only valid for observables that are insensitive to quasi-static offsets, i.e., the system's transfer function is negligibly small at low frequencies. However,

from the transfer function obtained (see Fig.3), one can see that this is not true. The system is susceptible to non-negligible perturbations even from small frequency noise.

V. WHITE NOISE ANALYSIS FOR THE ACCELERATION

Now we consider white noise for the external acceleration, i.e.

$$\mathcal{S}_{aa}(\omega) \equiv \mathcal{S}_{aa} = \text{constant} \quad (29)$$

Thus, the dephasing rate, using eq.(27) becomes:

$$\Gamma_{aa} = 4 \frac{\cos^2 \theta_0}{\omega_0^5} (\tilde{C}_R^2 + \tilde{C}_L^2) \times \frac{3\pi^2}{2} \mathcal{S}_{aa}. \quad (30)$$

For purpose of illustration, we consider a particular experimental setup with the magnetic field gradient, which determines the characteristic frequency, ω_0 , and τ , see eq.(4), to be $\eta_0 = 6 \times 10^3 \text{ Tm}^{-1}$, similar to values assumed in [30, 31, 65]. For a one-loop interferometer, the one-run experimental time is $\tau = 2\pi/\omega_0 \simeq 0.015\text{s}$ for a mass $m = 10^{-15}\text{kg}$ yields $\Delta x = 1\text{nm}$.

We further consider three scenarios: (a) The random acceleration fluctuation is along the interferometer axis where the magnitude of mean acceleration varies, (b) the external acceleration is assumed here to be zero ($a = 0 \text{ ms}^{-2}$). Further, we also consider the random acceleration fluctuations is at an arbitrary angle with respect to the interferometer axis, and (c) the mean acceleration is the gravitational acceleration, and $\theta_0 \sim 90^\circ$. Note that the upper bound on the total dephasing rate due to acceleration fluctuations from different sources can be computed using eq.(21).

A. Acceleration fluctuations along the interferometer axis

In Fig.4, we observe that the tolerable noise amplitude increases with decrease in magnitude of acceleration, a . This corroborates with eq.30, in the regime when the external force $ma \cos \theta_0 > C_j \eta_0$. However, when $ma \cos \theta_0 \approx C_j \eta_0$, the square root of the PSD acquires a maximum value for a fixed dephasing rate. Note that this value may change if we were to take higher order perturbations in the acceleration. For $\theta_0 = 0^\circ$, this is achieved for $a = a_m \sim 0.03 \text{ ms}^{-2}$. In particular, for $\Gamma\tau < 1$, we have the following bound on the noise amplitude spectral density:

$$\sqrt{\mathcal{S}_{aa}} < \mathcal{O}(10^{-8}) \text{ms}^{-2} \text{Hz}^{-1/2}, \text{ for } a = a_m = 0.03 \text{ ms}^{-2}.$$

For illustration only, we also present the bound on the acceleration noise amplitude under the constraint $\Gamma\tau <$

1, when the acceleration magnitude is $a = 3 \text{ ms}^{-2}$ and $\theta_0 = 0^\circ$:

$$\sqrt{\mathcal{S}_{aa}} < \mathcal{O}(10^{-13}) \text{ms}^{-2} \text{Hz}^{-1/2}, \text{ for } a = 3 \text{ms}^{-2}$$

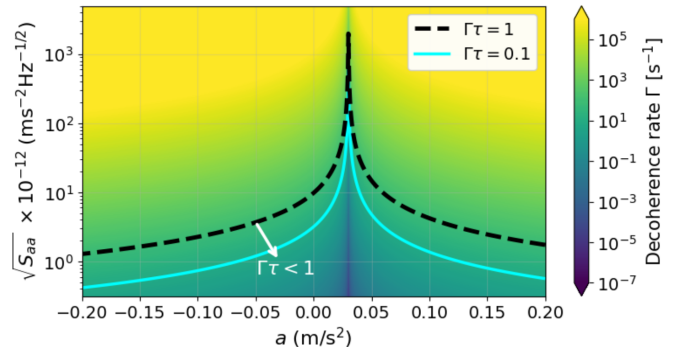


FIG. 4: The contour plots map the dephasing rate Γ as a function of the white noise amplitude spectral density $\sqrt{\mathcal{S}_{aa}}$ and the external acceleration magnitude a with all other parameters fixed to the values: $\theta_0 = 0^\circ$, $\eta_0 = 6 \times 10^3 \text{ Tm}^{-1}$, $m = 10^{-15} \text{ kg}$, $\tau = 2\pi/\omega_0 \simeq 0.015\text{s}$, which yields $\Delta x = 1\text{nm}$. The region below the black dashed contour corresponds to the experimentally desirable operating regime satisfying $\Gamma\tau < 1$. The graph shows that the behaviour of the dephasing rate and the tolerable square root of PSD, $\sqrt{\mathcal{S}_{aa}}$ is finite and smooth at $a_m \sim 0.03 \text{ ms}^{-2}$.

B. Arbitrary acceleration fluctuations with zero mean

We consider the setup when the mean acceleration is zero ($a = 0$) and the acceleration fluctuation both are along the interferometer axis. In Fig.5, we observe that the tolerable noise amplitude decreases with decrease in tilt angle, θ_0 . This corroborates with eq.30. This aligns with the physical intuition that when the acceleration fluctuations align along the interferometer axis, the dephasing is higher. While, if the acceleration fluctuations are perpendicular to the interferometer axis, the dynamics along the two axis decouple and hence ideally, no dephasing is expected. Hence, in the limit $\theta_0 \rightarrow 90^\circ$, we observe that an arbitrary noise amplitude is tolerable. However, this will not be the case, if we were to consider any dynamics of the nanodiamond in the direction of gravity.

In particular, for $\Gamma\tau < 1$, we have the following bound on the noise amplitude spectral density when the fluctuations are along the interferometer axis ($\theta_0 = 0^\circ$):

$$\Gamma\tau < 1 \implies \sqrt{\mathcal{S}_{aa}} < \mathcal{O}(10^{-11}) \text{ms}^{-2} \text{Hz}^{-1/2}.$$

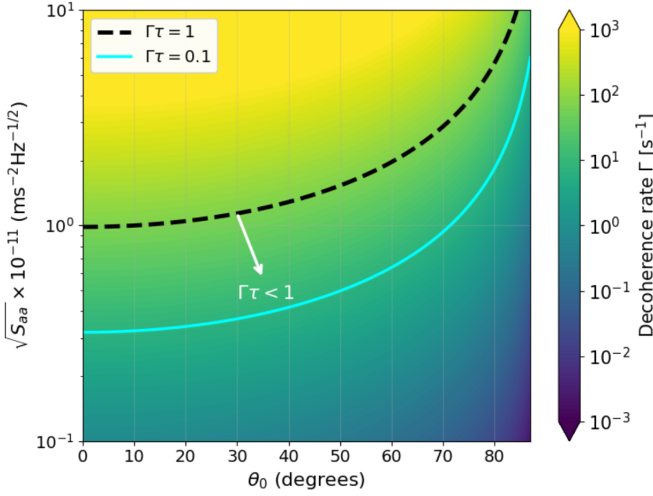


FIG. 5: The contour plot maps the dephasing rate Γ as a function of the white noise amplitude spectral density $\sqrt{\mathcal{S}_{aa}}$ and the tilt angle θ_0 with all other parameters fixed to the values: (no external acceleration) $a = 0\text{ms}^{-2}$, $\eta_0 = 6 \times 10^3\text{Tm}^{-1}$, $m = 10^{-15}\text{kg}$, $\Delta x = 1\text{nm}$, $\tau = 2\pi/\omega_0 \simeq 0.015\text{s}$. The region below the black dashed contour corresponds to the experimentally desirable operating regime satisfying $\Gamma\tau < 1$.

C. Gravitational fluctuations - Acceleration nearly perpendicular to interferometer axis

In general, we create the spatial superposition along an axis perpendicular to gravity. However, the interferometer axis may have a small tilt along the gravitational axis. In this subsection, we analyse the tolerable acceleration fluctuations along the gravitational axis.

In Fig.6, we observe that there is no constraint on the amplitude power spectral density when the acceleration fluctuations are perpendicular to the interferometer axis. This is because the dynamics and the fluctuations in the acceleration along the two axis decouple. However, for within a degree of deviation from the perpendicular orientation, we observe the following bound on $\sqrt{\mathcal{S}_{aa}}$ corresponding to the constraint $\Gamma < \tau^{-1}$, and $a = g = 9.81\text{ms}^{-2}$:

$$\begin{aligned} \sqrt{\mathcal{S}_{aa}} &< \mathcal{O}(10^{-10})\text{ms}^{-2}\text{Hz}^{-1/2} \quad \text{for } \theta_0 = 89^\circ \\ \sqrt{\mathcal{S}_{aa}} &< \mathcal{O}(10^{-6})\text{ms}^{-2}\text{Hz}^{-1/2} \quad \text{for } \theta_0 \sim 89.825^\circ \end{aligned}$$

We observe that the bound on the $\sqrt{\mathcal{S}_{aa}}$ changes by four orders of magnitude for a change within 1° of tilt angle. Thus, to operate in a regime where the system is less sensitive to the acceleration fluctuations, we need to fix the tilt angle between 89.8° and 90° .

In Fig.6, to the right of $\theta_0 \sim 89.825^\circ$, the magnetic force, $-(\chi_\rho m/\mu_0)B_0\eta_0$ dominates over external acceleration $ma \cos\theta_0$. Thus, between 89.9° and 90° , we can Taylor expand the dephasing rate expression given by eq.(30) with respect to theta, ignoring the external ac-

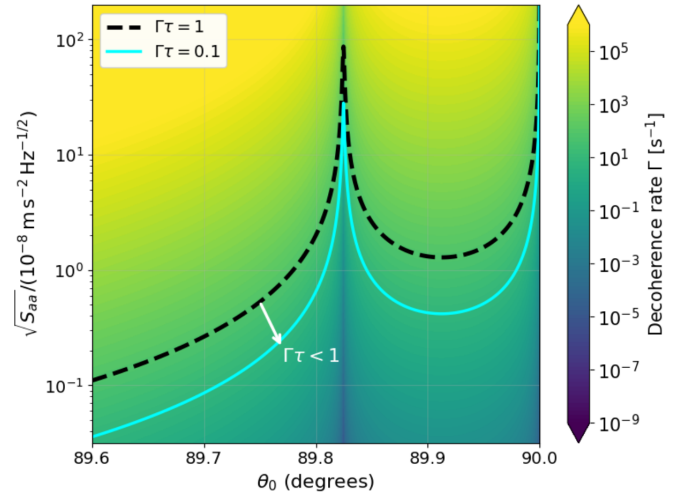


FIG. 6: The contour plots map the dephasing rate Γ as a function of the white noise amplitude spectral density $\sqrt{\mathcal{S}_{aa}}$ and the tilt angle θ_0 with all other parameters fixed to the values: $a = 9.81\text{ms}^{-2}$, $\eta_0 = 6 \times 10^3\text{Tm}^{-1}$, $m = 10^{-15}\text{kg}$, $\Delta x = 1\text{nm}$, $\tau = 2\pi/\omega_0 \simeq 0.015\text{s}$. The region below the black dashed contour corresponds to the experimentally desirable operating regime satisfying $\Gamma\tau < 1$. When the acceleration fluctuations are perpendicular to the interferometer axis ($\theta_0 = 90^\circ$), the dynamics along the two axes decouple and hence an arbitrary amplitude of $\sqrt{\mathcal{S}_{aa}}$ is tolerable at exactly $\theta_0 = 90^\circ$. The tolerable noise amplitude spectral density, $\sqrt{\mathcal{S}_{aa}}$ is finite and smooth at $\theta_0 \sim 89.825^\circ$, where a finite local minima in tolerance of the system to acceleration noise is achieved.

celeration term to obtain:

$$\Gamma_{aa} = \frac{4\theta_0^2}{\omega_0^5} (C_R^2 + C_L^2) \times \frac{3\pi^2}{2} \mathcal{S}_{aa}. \quad (31)$$

The sensitivity of the system to acceleration noise achieves a local minimum for $\theta_0 \sim 89.825^\circ$. This corresponds to θ_0 that minimizes $\tilde{C}_R^2 + \tilde{C}_L^2$ ⁹. In particular, this occurs when:

$$\tilde{C}_j = S_{x_j} \hbar \gamma_e \quad \text{when} \quad -\frac{\chi_\rho m}{\mu_0} B_0 \eta_0 = ma \sin \theta_0 \quad (32)$$

⁹Recall that: $C_j = \left(S_{x_j} \hbar \gamma_e - \frac{\chi_\rho m}{\mu_0} B_0 \right)$ and $\tilde{C}_j = C_j \eta_0 - ma \cos \theta_0$. We note that in the term C_j , $-(\chi_\rho m/\mu_0)B_0$ term is order of two times greater than $S_{x_j} \hbar \gamma_e$. Further, the former is interferometer arm independent, while the latter is interferometer arm dependent. Hence, minimizing \tilde{C}_j in eq.(7), corresponds to tuning $ma \cos \theta_0$ to cancel the contribution of $-(\chi_\rho m/\mu_0)B_0$. Physically, this occurs because the spin-independent magnetic force $(-\chi_\rho m/\mu_0)B_0\eta_0$ can be tuned to cancel the effective inertial force $(ma \sin \theta_0)$, yielding the net force along the interferometer axis to arise only from spin dependent force $S_{x_j} \hbar \gamma_e \eta_0$.

Conversely, if the the noise amplitude is $\sqrt{\mathcal{S}_{aa}} \sim \mathcal{O}(10^{-8})\text{ms}^{-2}\text{Hz}^{-1/2}$, the favorable operating regime is with $\theta_0 \in (89.8^\circ, 90^\circ)$.

VI. FLUCTUATIONS IN THE TILT OF THE INTERFEROMETER

Consider the fluctuation: $\theta_0 \rightarrow \theta_0 + \delta\theta(t)$. The procedure is similar to the previous section. The modified Lagrangian is:

$$\delta L_j = mx_j a_j \sin \theta_0 \delta\theta + \dots \quad (33)$$

where ... are due to trajectory and velocity fluctuations that do not contribute to dephasing in a one loop interferometer (refer Appendix.A). The corresponding fluctuation in the phase is:

$$\delta\phi = \frac{1}{\hbar} \int_0^\tau (\delta L_R - \delta L_L) dt \quad (34)$$

$$= \frac{ma}{\hbar} \sin \theta_0 \int_0^\tau \delta\theta(x_R - x_L) dt \quad (35)$$

where we consider $\tau = \frac{2\pi}{\omega_0}$ indicating a one loop interferometer. Similar to the previous section, we go to the Fourier basis:

$$\delta\theta(t) = \int_{-\infty}^{\infty} d\omega \delta\tilde{\theta}(\omega) e^{i\omega t} \quad (36)$$

Now we consider the fluctuations in θ_0 to follow gaussian noise statistics as given in eqs.(15)-(16).

$$E[\delta\tilde{\theta}_j(\omega)] = 0 \quad (37)$$

$$E[\delta\tilde{\theta}^*(\omega)\delta\tilde{\theta}(\omega')] = \mathcal{S}_{\theta\theta}(\omega)\delta(\omega - \omega') \quad (38)$$

where $\mathcal{S}_{\theta\theta}(\omega)$ is the PSD of the noise considered.

The dephasing rate is calculated using its relation to the second order correlation of the phase fluctuation:

$$\begin{aligned} \Gamma_{\theta\theta} &= E[\delta\phi^* \delta\phi] \\ &= \left(\frac{a \sin \theta_0}{\omega_0^2}\right)^2 (2\gamma_e \eta_0)^2 \int_0^\tau \int_0^\tau \int_{-\infty}^{\infty} \mathcal{S}_{\theta\theta}(\omega) \\ &\quad \times (\cos(\omega_0 t) - 1)(\cos(\omega_0 t') - 1) e^{i\omega(t-t')} dt' dt d\omega \end{aligned} \quad (39)$$

where $\Gamma_{\theta\theta}$ is the dephasing rate due to fluctuations in the tilt angle, θ_0 .

For small tilt angles, Eq. (39) suggests that the dephasing rate becomes negligible. However, this apparent suppression should be interpreted with caution: in this regime the approximation underlying the expression breaks down, because when the leading (first-order) dephasing contribution is small, higher-order effects fluctuations—can become non-negligible and may dominate the dephasing. However, in the analysis, while computing $\delta\phi^* \delta\phi$ in eq.(39), only the terms in the first order of fluctuations were retained.

Upon comparing the eq.(39) with the form in eq.(13), the effective transfer function is given by eq.(40).

$$\begin{aligned} |F_{\theta,\text{eff}}(\omega)|^2 &= \left(\frac{a \sin \theta_0}{\omega_0^2}\right)^2 (2\gamma_e \eta_0)^2 \int_0^\tau dt' \int_0^\tau dt \\ &\quad \times (\cos(\omega_0 t) - 1)(\cos(\omega_0 t') - 1) e^{i\omega(t-t')} \\ |F_{\theta,\text{eff}}(\omega_0 \xi)|^2 &= (4\gamma_e \eta_0)^2 \left(\frac{a \sin \theta_0}{\omega_0^3}\right)^2 \frac{\sin^2(\pi \xi)}{\xi^2(\xi^2 - 1)^2} \end{aligned} \quad (40)$$

We note that the behaviour of the part of the transfer function dependent on the noise frequency ω is the same as in eq.(28). Hence, the behaviour of the transfer function with respect to $\xi = \omega/\omega_0$ is explained by Fig.3. Only the scaling factors vary between the transfer functions corresponding to acceleration fluctuations and those corresponding to tilt fluctuations.

VII. WHITE NOISE ANALYSIS FOR THE TILT

We consider the case of white noise statistics with PSD given by:

$$\mathcal{S}_{\theta\theta}(\omega) = \mathcal{S}_{\theta\theta}. \quad (41)$$

Similar to the previous section, we consider a particular experimental setup with the magnetic field gradient, which determines the characteristic frequency, ω_0 , and T , see eq.(4), to be $\eta_0 = 6 \times 10^3 \text{Tm}^{-1}$, similar to values assumed in [30, 31, 65]. For a one-loop interferometer, the one-run experimental time is $\tau = 2\pi/\omega_0 \simeq 0.015\text{s}$ for a mass $m = 10^{-15}\text{kg}$.

In particular, we now consider the scenario where gravitational acceleration is perpendicular to the axis of spatial superposition ($\theta_0 = 90^\circ$) in the presence of tilt angle fluctuations with PSD $\mathcal{S}_{\theta\theta}$. The upper bound on $\sqrt{\mathcal{S}_{\theta\theta}}$ under the constraint that $\Gamma_{\theta\theta} \leq \omega_0/2\pi$ is given by:

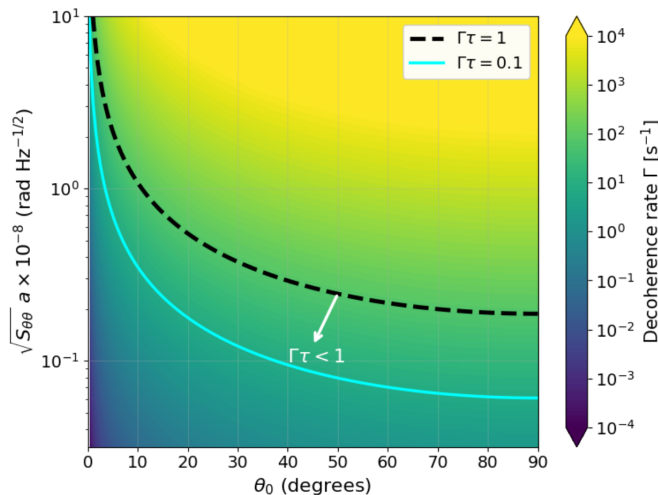
$$\sqrt{\mathcal{S}_{\theta\theta}} \lesssim \mathcal{O}(10^{-10}) \text{rad Hz}^{-1/2}$$

Now we shall probe the general trend of the upper bound on $\sqrt{\mathcal{S}_{\theta\theta}}$ for different values of random acceleration, a and for different values of tilt angle, θ_0 . We shall also probe the effect of varying the constraint on the coherence.

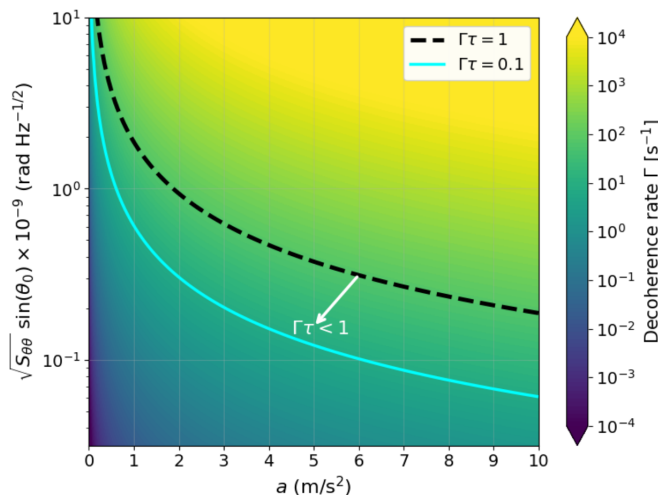
In Fig.7a, we observe that for a fixed dephasing rate and acceleration magnitude, with increase in the tilt angle, the constraint on $\sqrt{\mathcal{S}_{aa}}$ decreases. This corroborates with eq.(39), where the dephasing rate becomes maximum for $\theta_0 = 90^\circ$. Further, the order of magnitude of the bounds for different coherence constraints¹⁰, keeping all other parameters fixed, varies by at most one order of magnitude.

In Fig.7b, we see that the bound on $\sqrt{\mathcal{S}_{\theta\theta}}$ for a fixed dephasing rate and tilt angle, becomes stricter with increase in acceleration magnitude. Note that the acceleration dependence is introduced in the dephasing rate through the overall factor in eq.(39).

¹⁰A coherence measure of CM = 0.9 corresponds to $\Gamma\tau \sim 0.1$.



(a) For a fixed dephasing rate and acceleration magnitude, the upper bound on tolerable noise amplitude $\sqrt{\mathcal{S}_{\theta\theta}}$ loosens as the interferometer axis aligns with the direction of the applied acceleration (i.e., as $\theta_0 \rightarrow 0^\circ$). Note that the results close to 0° is not reliable since here, the second order effect of tilt fluctuations on the equation of motion become significant, however, this has not been considered in the present analysis.



(b) For a fixed dephasing rate, the upper bound on $\sqrt{\mathcal{S}_{\theta\theta}}$ becomes more stringent as the acceleration magnitude increases. In particular, for zero external acceleration, fluctuations in the tilt angle doesn't lead to dephasing.

FIG. 7: The contour plots map the dephasing rate Γ as a function of (a) $\sqrt{\mathcal{S}_{\theta\theta}} a$ and the tilt angle θ_0 , (b) $\sqrt{\mathcal{S}_{\theta\theta}} \sin(\theta_0)$ and acceleration a , with all other parameters fixed to the values: $\eta_0 = 6 \times 10^3 \text{Tm}^{-1}$, $m = 10^{-15} \text{kg}$, $\Delta x = 1 \text{nm}$, $\tau = 2\pi/\omega_0 \simeq 0.015 \text{s}$. The region below the black dashed contour corresponds to the regime satisfying $\Gamma\tau < 1$.

VIII. CONCLUSION

We have presented a quantitative noise analysis for fluctuations in random acceleration and in the tilt angle between the spatial superposition axis and the plane perpendicular to the acceleration in a matter-wave interferometer. We identified an operating regime in which the *spin-independent* contributions to the net force on each arm of the interferometer cancel. In this regime, the system is least susceptible to dephasing due to acceleration noise acting along the direction of the creation of the spatial superposition.

We showed how to quantitatively assess the fluctuations in (i) the random external acceleration a and (ii) the random choice in the tilt angle θ_0 that cause decoherence over many experimental runs. We did so by deriving the dephasing rate induced by these noise channels, under a statistical model for the fluctuations. The analysis was carried out in a Lagrangian framework: rather than introducing noise phenomenologically by assuming the transfer function, we treat the noise in the acceleration and the tilt angle individually as stochastic inputs in the action, compute the resulting stochastic phase difference between the two interferometer arms, and then obtain the dephasing rate by implementing the Wiener-Khinchin theorem [68, 69] for Gaussian noise statistics. This approach makes transparent (a) which physical terms in the dynamics are responsible for dephasing, and (b) how geometry and control parameters enter the susceptibility of the system to fluctuations. We then demonstrated the results for the case of white-noise statistics, i.e. constant power spectral densities for the acceleration and tilt fluctuations across frequency.

The bounds on the PSD are obtained by imposing a target coherence threshold $\Gamma\tau \leq 1$, where Γ is the dephasing rate and τ is the completion time for the one-loop interferometer in our particular setup, by fixing the values of system parameters according to ($\eta_0 = 6 \times 10^3 \text{Tm}^{-1}$, $m = 10^{-15} \text{kg}$, $\tau = 2\pi/\omega_0 \simeq 0.015 \text{s}$), which yields $\Delta x = 1 \text{nm}$ of spatial superposition. We tabulate the bounds on the PSD in Table.I).

For $\theta_0 = 0^\circ$, the operating regime with minimum sensitivity to noise is when $a_m = 0.03 \text{m s}^{-2}$. Similarly, when $a = 9.81 \text{m s}^{-2}$, the tilt angle for which the system has minimum sensitivity to external acceleration fluctuation is $\theta_m = 89.825^\circ$. However, note that upper bound on the acceleration noise parameter quickly becomes stricter in the vicinity of the minimum sensitivity regions.

We also computed the bound on the PSD of the tilt angle, when the gravitational acceleration ($a = 9.81 \text{m s}^{-2}$) is acting perpendicular to the spatial superposition, and obtained the following bound to satisfy the coherence constraint of $\Gamma\tau < 1$: $\sqrt{\mathcal{S}_{\theta\theta}} \lesssim \mathcal{O}(10^{-10}) \text{rad Hz}^{-1/2}$.

We showed that the bound on acceleration-noise $\sqrt{\mathcal{S}_{aa}}$ becomes progressively stricter as the axis of spatial superposition aligns with the direction of the external random acceleration. However, the bound on tilt-noise $\sqrt{\mathcal{S}_{\theta\theta}}$ decreases with the alignment along the acceleration di-

TABLE I: We denote the bounds on the square root of the PSD for the parameters $m = 10^{-15}$ kg, $\Delta x = 1$ nm, and $\tau = 0.015$ s, where a denotes the external acceleration to the interferometer and θ_0 is the angle between the spatial superposition axis and the acceleration noise. We emphasize that the values of a_m and θ_m —which mark regimes in which the system is comparatively less susceptible to acceleration noise—depend on other experimental parameters; the values quoted here are provided for illustrative purposes. For the discussion on a_m , see Fig. 4, and θ_m , see Fig. 6. We should cautiously approach the values mentioned below for a_m , θ_m . These are based on the choice of the parameters, and also they demand higher order corrections, which we have not taken in our current analysis.

θ_0 (deg)	a (m s^{-2})	$\sqrt{\mathcal{S}_{aa}}$ ($\text{m s}^{-2} \text{Hz}^{-1/2}$)
0	$a_m = 0.03$	$\mathcal{O}(10^{-8})$
0	0	$\mathcal{O}(10^{-11})$
0	3	$\mathcal{O}(10^{-13})$
89	9.81	$\mathcal{O}(10^{-10})$
$\theta_m = 89.825$	9.81	$\mathcal{O}(10^{-6})$

rection, for a fixed dephasing rate.

Finally, while the white-noise assumption provides a clean and conservative baseline for requirements, realistic environments are often colored (frequency-dependent)

and may exhibit correlations between arms. The Lagrangian framework developed here is naturally extensible to such scenarios by replacing the flat PSD with measured or modelled spectra and by incorporating cross-correlators to characterise the noise source and, hence, estimate the dephasing.

ACKNOWLEDGMENTS

We would like to thank Tracy Northup for the discussions related to the acceleration noise in the experimental setup. A.M.'s, S.B.'s and A.G.'s research is funded by the Gordon and Betty Moore Foundation through Grant GBMF12328, DOI 10.37807/GBMF12328. This material is based on work supported by the Alfred P. Sloan Foundation under Grant No. G-2023-21130. A.G. also acknowledges support from NSF grants PHY-2409472 and PHY-2111544, DARPA, the John Templeton Foundation, the W.M. Keck Foundation, and the Simons Foundation. SNM would like to thank the organizers of the workshop, Schrodinger Cats: The quest to find the edge of the quantum world, held at OIST, Japan for facilitating academic interactions that led to this collaboration. SNM acknowledges support from the Kishore Vaigyanik Protsahan Yojana (KVPY) fellowship, SX-2011055, awarded by the Department of Science and Technology, Government of India. SB would like to acknowledge EPSRC grants (EP/N031105/1, EP/S000267/1, and EP/X009467/1) and grant ST/W006227/1.

-
- [1] R. Colella, A. W. Overhauser, and S. A. Werner, Observation of gravitationally induced quantum interference, *Phys. Rev. Lett.* **34**, 1472 (1975).
- [2] S. A. Werner, J. L. Staudenmann, and R. Colella, EFFECT OF EARTH'S ROTATION ON THE QUANTUM MECHANICAL PHASE OF THE NEUTRON, *Phys. Rev. Lett.* **42**, 1103 (1979).
- [3] H. Rauch and S. A. Werner, *Neutron Interferometry : Lessons in Experimental Quantum Mechanics, Second Edition* (Oxford University Press, 2015).
- [4] J. B. Fixler, G. T. Foster, J. M. McGuirk, and M. A. Kasevich, Atom interferometer measurement of the Newtonian constant of gravity, *Science* **315**, 74 (2007).
- [5] P. Asenbaum, C. Overstreet, T. Kovachy, D. D. Brown, J. M. Hogan, and M. A. Kasevich, Phase Shift in an Atom Interferometer due to Spacetime Curvature across its Wave Function, *Phys. Rev. Lett.* **118**, 183602 (2017), arXiv:1610.03832 [physics.atom-ph].
- [6] C. Overstreet, P. Asenbaum, J. Curti, M. Kim, and M. A. Kasevich, Observation of a gravitational Aharonov-Bohm effect, *Science* **375**, abl7152 (2021).
- [7] O. Amit, Y. Margalit, O. Dobkowski, Z. Zhou, Y. Japha, M. Zimmermann, M. A. Efremov, F. A. Narducci, E. M. Rasel, W. P. Schleich, and R. Folman, T^3 stern-gerlach matter-wave interferometer, *Phys. Rev. Lett.* **123**, 083601 (2019).
- [8] Y. Margalit, O. Dobkowski, Z. Zhou, O. Amit, Y. Japha, S. Moukouri, D. Rohrlrich, A. Mazumdar, S. Bose, C. Henkel, and R. Folman, Realization of a complete stern-gerlach interferometer: Toward a test of quantum gravity, *Science Advances* **7**, eabg2879 (2021).
- [9] T. Kovachy, Quantum superposition at the half-metre scale, et.al, *Nature* **528**, 530–533 (2015).
- [10] M. Arndt, Wave-particle duality of c(60) molecules, et.al., *Nature* **680** (1999).
- [11] S. Eibenberger, S. Gerlich, M. Arndt, M. Mayor, and J. Tüxen, Matter-wave interference with particles selected from a molecular library with masses exceeding 10000 amu, *Phys. Chem. Chem. Phys.* **15**, 14696 (2013), arXiv:1310.8343 [quant-ph].
- [12] Y. Y. Fein, P. Geyer, P. Zwick, F. Kiałka, S. Pedalino, M. Mayor, S. Gerlich, and M. Arndt, Quantum superposition of molecules beyond 25 kDa, *Nature Phys.* **15**, 1242 (2019).
- [13] S. Pedalino, B. E. Ramírez-Galindo, R. Ferstl, K. Hornberger, M. Arndt, and S. Gerlich, Probing quantum mechanics using nanoparticle schrödinger cats (2025), arXiv:2507.21211 [quant-ph].
- [14] M. Arndt and K. Hornberger, Testing the limits of quantum mechanical superpositions, *Nature Physics* **10**, 271

- (2014).
- [15] S. Bose, A. Mazumdar, G. W. Morley, H. Ulbricht, M. Toroš, M. Paternostro, A. Geraci, P. Barker, M. S. Kim, and G. Milburn, Spin Entanglement Witness for Quantum Gravity, *Phys. Rev. Lett.* **119**, 240401 (2017), arXiv:1707.06050 [quant-ph].
- [16] https://www.youtube.com/watch?v=0Fv-0k13s_k (2016), accessed 1/11/22.
- [17] C. Marletto and V. Vedral, Gravitationally induced entanglement between two massive particles is sufficient evidence of quantum effects in gravity, *Phys. Rev. Lett.* **119**, 240402 (2017).
- [18] D. Biswas, S. Bose, A. Mazumdar, and M. Toroš, Gravitational optomechanics: Photon-matter entanglement via graviton exchange, *Phys. Rev. D* **108**, 064023 (2023), arXiv:2209.09273 [gr-qc].
- [19] S. G. Elahi, M. Schut, A. Dana, A. Grinin, S. Bose, A. Mazumdar, and A. Geraci, Diamagnetic microchip traps for levitated nanoparticle entanglement experiments, arXiv preprint arXiv:2411.02325 (2024), arXiv:2411.02325 [quant-ph].
- [20] U. K. Beckerling Vinckers, Á. De La Cruz-Dombriz, and A. Mazumdar, Quantum entanglement of masses with nonlocal gravitational interaction, *Physical Review D* **107**, 124036 (2023).
- [21] S. Chakraborty, A. Mazumdar, and R. Pradhan, Distinguishing jordan and einstein frames in gravity through entanglement, *Physical Review D* **108**, L121505 (2023).
- [22] S. Bose, A. Mazumdar, M. Schut, and M. Toroš, Entanglement Witness for the Weak Equivalence Principle, *Entropy* **25**, 448 (2023), arXiv:2203.11628 [gr-qc].
- [23] A. Bassi, K. Lochan, S. Satin, T. P. Singh, and H. Ulbricht, Models of wave-function collapse, underlying theories, and experimental tests, *Rev. Mod. Phys.* **85**, 471 (2013).
- [24] O. Romero-Isart, A. C. Pflanzer, F. Blaser, R. Kaltenbaek, N. Kiesel, M. Aspelmeyer, and J. I. Cirac, Large quantum superpositions and interference of massive nanometer-sized objects., *Physical review letters* **107**, 020405 (2011).
- [25] T. W. van de Kamp, R. J. Marshman, S. Bose, and A. Mazumdar, Quantum Gravity Witness via Entanglement of Masses: Casimir Screening, *Phys. Rev. A* **102**, 062807 (2020), arXiv:2006.06931 [quant-ph].
- [26] M. Schut, J. Tilly, R. J. Marshman, S. Bose, and A. Mazumdar, Improving resilience of quantum-gravity-induced entanglement of masses to decoherence using three superpositions, *Phys. Rev. A* **105**, 032411 (2022), arXiv:2110.14695 [quant-ph].
- [27] M. Schut, P. Andriolo, M. Toroš, S. Bose, and A. Mazumdar, Decoherence rate expression due to air molecule scattering in spatial qubits, arXiv preprint arXiv:2410.20910 (2024), arXiv:2410.20910 [quant-ph].
- [28] S. Rijavec, M. Carlesso, A. Bassi, V. Vedral, and C. Marletto, Decoherence effects in non-classicality tests of gravity, *New J. Phys.* **23**, 043040 (2021), arXiv:2012.06230 [quant-ph].
- [29] M. Schut, A. Grinin, A. Dana, S. Bose, A. Geraci, and A. Mazumdar, Relaxation of experimental parameters in a quantum-gravity-induced entanglement of masses protocol using electromagnetic screening, *Phys. Rev. Res.* **5**, 043170 (2023), arXiv:2307.07536 [quant-ph].
- [30] S. N. Moorthy, A. Geraci, S. Bose, and A. Mazumdar, Magnetic noise in macroscopic quantum spatial superpositions, *Phys. Rev. A* **112**, 022416 (2025), arXiv:2504.13252 [quant-ph].
- [31] S. N. Moorthy and A. Mazumdar, Magnetic noise in macroscopic quantum spatial superposition induced by inverted harmonic oscillator potential (2025), arXiv:2509.02670 [quant-ph].
- [32] P. Fragolino, M. Schut, M. Toroš, S. Bose, and A. Mazumdar, Decoherence of a matter-wave interferometer due to dipole-dipole interactions, *Phys. Rev. A* **109**, 033301 (2024), arXiv:2307.07001 [quant-ph].
- [33] D. Leibfried, R. Blatt, C. Monroe, and D. Wineland, Quantum dynamics of single trapped ions, *Rev. Mod. Phys.* **75**, 281 (2003).
- [34] M. Toroš, T. W. Van De Kamp, R. J. Marshman, M. S. Kim, A. Mazumdar, and S. Bose, Relative acceleration noise mitigation for nanocrystal matter-wave interferometry: Applications to entangling masses via quantum gravity, *Phys. Rev. Res.* **3**, 023178 (2021), arXiv:2007.15029 [gr-qc].
- [35] M.-Z. Wu, M. Toroš, S. Bose, and A. Mazumdar, Inertial torsion noise in matter-wave interferometers for gravity experiments, *Physical Review D* **111**, 064004 (2025).
- [36] C. Henkel and R. Folman, Internal decoherence in nano-object interferometry due to phonons, *AVS Quantum Sci.* **4**, 025602 (2022), arXiv:2112.01263 [quant-ph].
- [37] C. Henkel and R. Folman, Universal limit on spatial quantum superpositions with massive objects due to phonons, *Phys. Rev. A* **110**, 042221 (2024), arXiv:2305.15230 [quant-ph].
- [38] Q. Xiang, R. Zhou, S. Bose, and A. Mazumdar, Phonon Induced Contrast in Matter Wave Interferometer, *Phys. Rev. A* **110**, 042614 (2024), arXiv:2404.04210 [quant-ph].
- [39] B. A. Stickler, K. Hornberger, and M. S. Kim, Quantum rotations of nanoparticles, *Nature Rev. Phys.* **3**, 589 (2021), arXiv:2102.00992 [quant-ph].
- [40] B. A. Stickler, B. Papendell, S. Kuhn, B. Schirnski, J. Millen, M. Arndt, and K. Hornberger, Probing macroscopic quantum superpositions with nanorotors, *New J. Phys.* **20**, 122001 (2018), arXiv:1803.01778 [quant-ph].
- [41] C. C. Rusconi, M. Perdriat, G. Hétet, O. Romero-Isart, and B. A. Stickler, Spin-Controlled Quantum Interference of Levitated Nanorotors, *Phys. Rev. Lett.* **129**, 093605 (2022), arXiv:2203.11717 [quant-ph].
- [42] Y. Japha and R. Folman, Quantum Uncertainty Limit for Stern-Gerlach Interferometry with Massive Objects, *Phys. Rev. Lett.* **130**, 113602 (2023), arXiv:2202.10535 [quant-ph].
- [43] T. Zhou, S. Bose, and A. Mazumdar, Gyroscopic stability for nanoparticles in Stern-Gerlach Interferometry and spin contrast, arXiv preprint arXiv:2407.15813 (2024), arXiv:2407.15813 [quant-ph].
- [44] R. Rizaldy, T. Zhou, S. Bose, and A. Mazumdar, Rotational stability in nanorotor and spin contrast in one-loop interferometry in the Stern-Gerlach setup, arXiv preprint arXiv:2412.15335 (2024), arXiv:2412.15335 [quant-ph].
- [45] O. Romero-Isart, Quantum superposition of massive objects and collapse models, *Phys. Rev. A* **84**, 052121 (2011).
- [46] K. Hornberger, S. Gerlich, P. Haslinger, S. Nimmrichter, and M. Arndt, Colloquium: Quantum interference of clusters and molecules, *Reviews of Modern Physics* **84**, 157 (2012).
- [47] B. Englert, J. Schwinger, and M. O. Scully, Is spin coher-

- ence like humpty-dumpty? i. simplified treatment, *Foundations of Physics* **18**, 1045 (1988).
- [48] J. Schwinger, M. O. Scully, and B. G. Englert, Is spin coherence like Humpty-Dumpty?, *Zeitschrift fur Physik D Atoms Molecules Clusters* **10**, 135 (1988).
- [49] M. O. Scully, B.-G. Englert, and J. Schwinger, Spin coherence and humpty-dumpty. iii. the effects of observation, *Phys. Rev. A* **40**, 1775 (1989).
- [50] Y. Margalit, O. Dobkowski, Z. Zhou, O. Amit, Y. Japha, S. Moukouri, D. Rohrllich, A. Mazumdar, S. Bose, C. Henkel, and R. Folman, Realization of a complete stern-gerlach interferometer: Towards a test of quantum gravity, *Science Advances* **7**, 10.1126/sciadv.abg2879 (2021).
- [51] M. W. Doherty, N. B. Manson, P. Delaney, F. Jelezko, J. Wrachtrup, and L. C. Hollenberg, The nitrogen-vacancy colour centre in diamond, *Physics Reports* **528**, 1–45 (2013).
- [52] U. Delić, M. Reisenbauer, K. Dare, D. Grass, V. Vuletić, N. Kiesel, and M. Aspelmeyer, Cooling of a levitated nanoparticle to the motional quantum ground state, *Science* **367**, 892 (2020).
- [53] J. Piotrowski, D. Windey, J. Vijayan, C. Gonzalez-Ballester, A. de los Ríos Sommer, N. Meyer, R. Quidant, O. Romero-Isart, R. Reimann, and L. Novotny, Simultaneous ground-state cooling of two mechanical modes of a levitated nanoparticle, *Nature Physics* **19**, 1009 (2023).
- [54] M. Kamba, R. Shimizu, and K. Aikawa, Nanoscale feedback control of six degrees of freedom of a near-sphere, *Nature Commun.* **14**, 7943 (2023), arXiv:2303.02831 [physics.optics].
- [55] D. S. Bykov, L. Dania, F. Goschin, and T. E. Northup, 3D sympathetic cooling and detection of levitated nanoparticles, *Optica* **10**, 438 (2023), arXiv:2210.07583 [physics.optics].
- [56] M. Perdriat, C. C. Rusconi, T. Delord, P. Huillery, C. Pellet-Mary, A. Durand, B. A. Stickler, and G. Hézet, Rotational Locking of Charged Microparticles in Quadrupole Ion Traps, *Phys. Rev. Lett.* **133**, 253602 (2024).
- [57] J.-F. Hsu, P. Ji, C. W. Lewandowski, and B. D’Urso, Cooling the motion of diamond nanocrystals in a magneto-gravitational trap in high vacuum, *Scientific reports* **6**, 30125 (2016).
- [58] S. A. Hughes and K. S. Thorne, Seismic gravity-gradient noise in interferometric gravitational-wave detectors, *Physical Review D* **58**, 10.1103/physrevd.58.122002 (1998).
- [59] P. R. Saulson, Terrestrial gravitational noise on a gravitational wave antenna, *Phys. Rev. D* **30**, 732 (1984).
- [60] K. S. Thorne and C. J. Winstein, Human gravity-gradient noise in interferometric gravitational-wave detectors, *Physical Review D* **60**, 10.1103/physrevd.60.082001 (1999).
- [61] J. Harms, Terrestrial gravity fluctuations, *Living Reviews in Relativity* **22**, 10.1007/s41114-019-0022-2 (2019).
- [62] M. Schut, A. Geraci, S. Bose, and A. Mazumdar, Micrometer-size spatial superpositions for the QGEM protocol via screening and trapping, *Phys. Rev. Res.* **6**, 013199 (2024), arXiv:2307.15743 [quant-ph].
- [63] M. Schut and A. Mazumdar, Parameter scanning in a quantum-gravity-induced entanglement of masses (QGEM) experiment with electromagnetic screening (2025), arXiv:2502.12474 [quant-ph].
- [64] J. S. Pedernales, G. W. Morley, and M. B. Plenio, Motional Dynamical Decoupling for Interferometry with Macroscopic Particles, *Phys. Rev. Lett.* **125**, 023602 (2020).
- [65] R. J. Marshman, A. Mazumdar, R. Folman, and S. Bose, Constructing nano-object quantum superpositions with a Stern-Gerlach interferometer, *Phys. Rev. Res.* **4**, 023087 (2022), arXiv:2105.01094 [quant-ph].
- [66] A. Gruber, A. Dräbenstedt, C. Tietz, L. Fleury, J. Wrachtrup, and C. von Borczyskowski, Scanning confocal optical microscopy and magnetic resonance on single defect centers, *Science* **276**, 2012 (1997), <https://www.science.org/doi/pdf/10.1126/science.276.5321.2012>.
- [67] P. W. Bowen and J. G. Milburn, *Quantum Optomechanics* (CRC Press, Boca Raton, 2015).
- [68] N. Wiener, Generalized harmonic analysis, *Acta Mathematica* **55**, 117 (1930).
- [69] A. Khintchine, Korrelationstheorie der stationären stochastischen prozesse, *Mathematische Annalen* **109**, 604 (1934).
- [70] M.-Z. Wu, Acceleration Noise Induced Decoherence in Stern-Gerlach Interferometers for Gravity Experiments (2024), arXiv:2406.10832 [quant-ph].

Appendix A: Contribution of trajectory and velocity fluctuations to dephasing

Consider a Lagrangian $\mathcal{L}(\dot{x}, x, t)$. The equation of motion is then given by:

$$\frac{d}{dt} \frac{\partial \mathcal{L}}{\partial \dot{x}} - \frac{\partial \mathcal{L}}{\partial x} = 0 \quad (\text{A1})$$

Consider the fluctuation in the the Lagrangian, $\delta \mathcal{L}$ introduced by some noise source $\delta \zeta$.

$$\delta \mathcal{L} = \frac{\partial \mathcal{L}}{\partial \dot{x}} \delta \dot{x} + \frac{\partial \mathcal{L}}{\partial x} \delta x + \frac{\partial \mathcal{L}}{\partial \zeta} \delta \zeta \quad (\text{A2})$$

Substituting for $\frac{\partial \mathcal{L}}{\partial \dot{x}}$ from eq.(A1) in eq.(A2), we obtain:

$$\begin{aligned} \delta \mathcal{L} &= \frac{\partial \mathcal{L}}{\partial \dot{x}} \delta \dot{x} + \frac{d}{dt} \frac{\partial \mathcal{L}}{\partial \dot{x}} \delta x + \frac{\partial \mathcal{L}}{\partial \zeta} \delta \zeta \\ &= \frac{d}{dt} \left(\frac{\partial \mathcal{L}}{\partial \dot{x}} \delta x \right) + \frac{\partial \mathcal{L}}{\partial \zeta} \delta \zeta \end{aligned} \quad (\text{A3})$$

Consider $\delta \phi$ arising from $\delta \mathcal{L}$:

$$\begin{aligned} \delta \phi &= \frac{1}{\hbar} \int_0^T dt \delta \mathcal{L}(\dot{x}, x, t) \\ &= \frac{1}{\hbar} \int_0^T dt \left[\frac{d}{dt} \left(\frac{\partial \mathcal{L}}{\partial \dot{x}} \delta x \right) + \frac{\partial \mathcal{L}}{\partial \zeta} \delta \zeta \right] \end{aligned} \quad (\text{A4})$$

where $T = \frac{2\pi}{\omega_0}$. $\delta x(t)$ is defined upto its statistical properties deriving from the statistical properties of $\delta \zeta$ and the modified equations of motion. However, for each experimental run, $\delta x(t)$ will be a continuous and differentiable function, since it is describing the classical trajectory of a particle. Hence, we can apply the fundamental theorem of calculus (FTC). Now imposing the FTC on the first term, we obtain:

$$\delta \phi = \frac{1}{\hbar} \left(\frac{\partial \mathcal{L}}{\partial \dot{x}} \delta x \right) \Big|_{t=0}^{t=T} + \frac{1}{\hbar} \int_0^T dt \frac{\partial \mathcal{L}}{\partial \zeta} \delta \zeta \quad (\text{A5})$$

Now we consider the following type of Lagrangian:

$$\mathcal{L}(\dot{x}, x, t) = \frac{1}{2} A \dot{x}^2 - V(x, t) \quad (\text{A6})$$

where A is a constant, and $V(x, t)$ is a function of position and time, independent of velocity. Thus,

$$\frac{\partial \mathcal{L}}{\partial \dot{x}} \delta x = A \dot{x} \delta x \quad (\text{A7})$$

In a one loop interferometer, $\dot{x}(T) = 0 = \dot{x}(0)$. Thus, the first term in eq.(A5) vanishes. This tells us that the phase fluctuation arises only from the direct fluctuation of acceleration and not from the induced trajectory and the velocity perturbations.

Appendix B: Remarks on correlation statistics

For processes $A(t), B(t)$ define the cross-correlation by

$$R_{AB}(\tau) \equiv \mathbb{E}[A(t+\tau) B^*(t)], \quad (\text{B1})$$

and the corresponding (cross-)power spectral density (PSD) by the Fourier transform

$$S_{AB}(\omega) \equiv \int_{-\infty}^{\infty} d\tau e^{i\omega\tau} R_{AB}(\tau). \quad (\text{B2})$$

Let

$$Z(t) = X(t) - Y(t). \quad (\text{B3})$$

Then the autocorrelation of Z is

$$\begin{aligned} R_{ZZ}(\tau) &= \mathbb{E}[(X(t+\tau) - Y(t+\tau))(X^*(t) - Y^*(t))] \\ &= \mathbb{E}[X(t+\tau)X^*(t)] + \mathbb{E}[Y(t+\tau)Y^*(t)] \\ &\quad - \mathbb{E}[X(t+\tau)Y^*(t)] - \mathbb{E}[Y(t+\tau)X^*(t)] \\ &= R_{XX}(\tau) + R_{YY}(\tau) - R_{XY}(\tau) - R_{YX}(\tau). \end{aligned} \quad (\text{B4})$$

Fourier transforming term-by-term gives

$$S_{ZZ}(\omega) = S_{XX}(\omega) + S_{YY}(\omega) - S_{XY}(\omega) - S_{YX}(\omega). \quad (\text{B5})$$

For wide sense stationary processes, the kind that we assume in this paper, one has $S_{YX}(\omega) = S_{XY}^*(\omega)$. Hence

$$S_{ZZ}(\omega) = S_{XX}(\omega) + S_{YY}(\omega) - 2 \operatorname{Re}\{S_{XY}(\omega)\}. \quad (\text{B6})$$

If X and Y are uncorrelated if and only if $\operatorname{Re}\{S_{XY}(\omega)\} = 0$. Then the effective power spectral density is just the some of the PSD of each, X and Y . If $\operatorname{Re}\{S_{XY}(\omega)\} < 0$, then the fluctuations between X and Y are anti-correlated. This increases the effective power spectral density more than the uncorrelated case. If $\operatorname{Re}\{S_{XY}(\omega)\} > 0$, then the two variables are correlated, and the effective PSD is lesser than the uncorrelated case. Note that the autocorrelation power spectral density ($S_{XX}(\omega)$ & $S_{YY}(\omega)$) is positive semi-definite.

In case of an interferometer dephasing, we consider the differential phase fluctuations (i.e., $\delta \phi = \frac{1}{\hbar} \int_0^T dt (L_R - L_L) \equiv \delta \phi_R - \delta \phi_L$). Hence, the effective PSD can be modelled as given in eq.(B6). We argue that in case of the noise correlation between the arms of a Stern-Gerlach type interferometer, is a positive correlation (Refer footnote(8)). Thus, computing the dephasing rate under the assumption of uncorrelated fluctuations imposes an upper bound on it. Similar conclusions were brought in a slightly different context in [35].